Q. J. R. Meteorol. Soc. (2002), **submitted**, pp. 1–18

Comparative Analysis of Rainfall in MAP Cases IOP2B and IOP8

By RICHARD ROTUNNO[1]* and ROSSELLA FERRETTI[2]

[1]*National Center for Atmospheric Research*†*, USA*
[2]*Department of Physics, University of L'Aquila, Via Vetoio, 67010 Coppito-L'Aquila, Italy*

(Submitted 31 January 2002)

SUMMARY

Although the large-scale flow was similar, important differences in mesoscale atmospheric structure made the difference between moderately intense rain in IOP2B and relatively light rain in IOP8 in the Lago Maggiore Target Area (LMTA). This conclusion is supported here through analysis of data from, and numerical simulations of, these two cases. Analysis of the large-scale data show that there was in both cases a moist tongue of southerly flow moving from west to east of the Alpine south side. Mesoscale data analysis and numerical simulations suggest that the most important difference between the two cases was the presence of a cold stable air mass in the Po Valley in IOP8 which persisted through the period in which the large-scale moist tongue was progressing eastward and prevented the most humid air from reaching the LMTA. Another difference contributing to the greater rainfall in the LMTA in IOP2B was the development of conditional instability (with associated convective rain) due to the effect of the Alps on the eastward passage of the moist tongue; in IOP8 the atmosphere remained locally stable throughout the period.

KEYWORDS: Mesoscale Alpine Programme Orographic Rain Blocking

1. INTRODUCTION

Improved understanding of the influence of orography on precipitation was one of the principle scientific objectives of the Mesoscale Alpine Programme (MAP; Bougeault *et al.* 2000). The main focus of the precipitation-related part of the MAP Special Observing Period (SOP; 7 September – 15 November 1999) was the climatologically favored Lago Maggiore Target Area (LMTA) on the south side of the northwestern Alps (Fig. 1). Studies of previous heavy rain events on the Alpine south side showed the importance of deep and slowly progressive upper-level troughs with associated moist southerly flow (e.g. Massacand et al. 1998; Doswell *et al.* 1998). Expectations based on the latter, and on real-time forecasts, lead to roughly thirteen of the eighteen Intensive Observation Periods (IOPs) being chosen with study of precipitation in the LMTA as an objective (see Table 5 of Bougeault *et al.* 2000). The degree to which the observed rainfall conformed to the expectations for heavy rain varied among these roughly thirteen cases. In the present paper we analyze data taken during the MAP SOP, supplemented by numerical simulations, to compare the case that came closest to (IOP2B, 19 – 20 September 1999) with the case that was furthest from (IOP8, 20 – 21 October 1999) the expectations for heavy rain in the LMTA.

Figure 2 both introduces and summarizes the findings of the present study. As in previous heavy rain cases on the Alpine south side, in both IOP2B and IOP8 there were precursor upper-level troughs (Figs. 2a-b) with associated moist southerly flow at low levels (Figs. 2c-d). The numerical forecast models called for major rain events for the LMTA in both cases (see MAP Field Catalog, POC Science Coordinator Notes, available at http://www.map.ethz.ch); heavy rain occurred in IOP2B, but there was only light rain in IOP8. The central theme of our analysis is that the relatively poor forecast and the occurrence of light rain in IOP8 were due to the presence of a deep layer of cold air in northwestern Italy [evidenced in Fig. 2d by the blocked southerly flow in the Gulf of

* Corresponding author address: Richard Rotunno, NCAR PO BOX 3000, Boulder CO, USA. E-mail: rotunno@ucar.edu

† National Center for Atmospheric Research is sponsored by the National Science Foundation

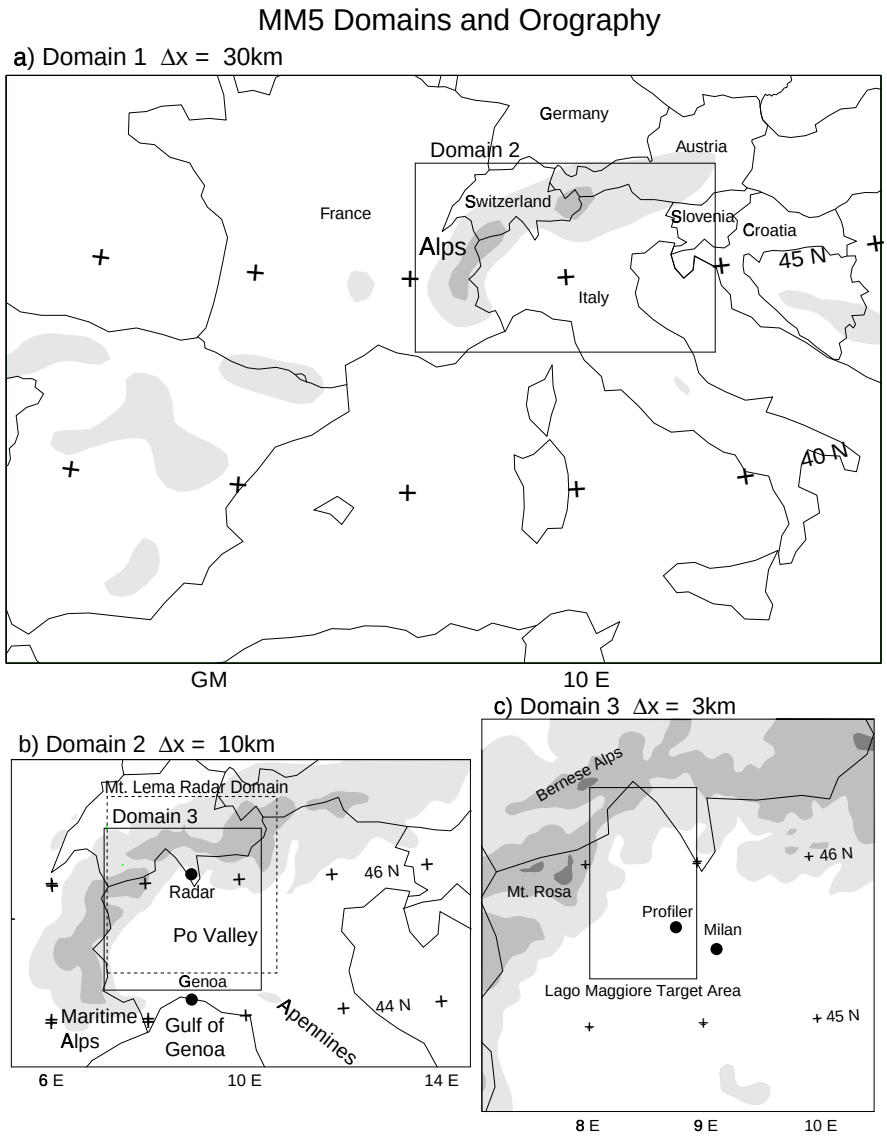

Figure 1. Domains for numerical simulations used in this study showing orography (light shading > 1 km; darker shading > 2 km; darkest shading > 3 km) centered on a) Europe, with countries containing the Alps named, b) the Alps, and c) northwestern Italy, with geographical and other locations indicated.

Genoa (Fig. 1b)], which was detected late by the models, and which prevented moisture-laden air from reaching the LMTA.

The coarse-grain view of orographic flow modification (Fig. 2) is brought into clearer focus here with an analysis of the data taken during the MAP SOP. In the following section, we present a side-by-side analysis of IOP2B and IOP8 with respect to precipitation (rain gauge and radar data), thermodynamic structure (soundings), and wind (soundings and wind profiler data).

In Section 3 we present an analysis of numerical simulations of IOP2B and IOP8 using the fifth-generation NCAR/Penn State Mesoscale Model (MM5), version 2.12. Taken

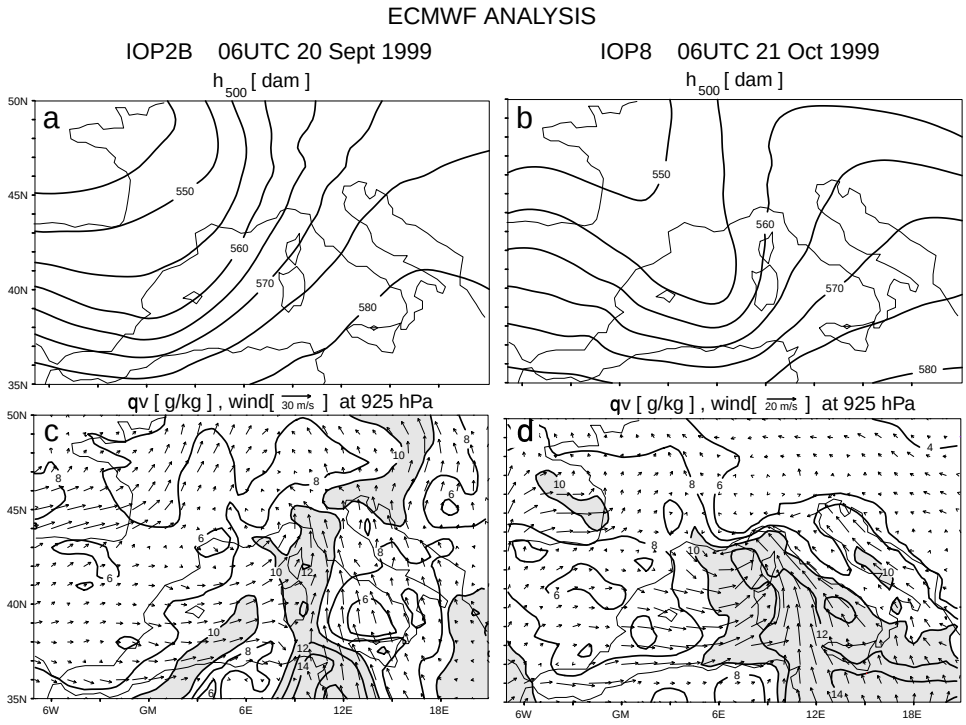

Figure 2. Analysis from the European Center for Medium Range Forecasting (ECMWF) of 500 hPa heights (c.i. = 5 dam) at a) 06UTC 20 September 1999 and b) 06UTC 21 October 1999, and 925 hPa wind and water vapor mixing ratio (c.i. = 2 g/kg) at c) 06UTC 20 September 1999 and d) 06UTC 21 October 1999.

together the MAP SOP data and numerical simulations suggest the following interpretation of the difference in rainfall between the two cases: In both cases there was a moist tongue of southerly flow (Figs. 2c-d) moving from west to east of northern Italy. The model results support the idea that the most important difference between the cases was the presence of a cold stable air mass in the Po Valley (Fig. 1b) in IOP8 which persisted through the period in which the large-scale moist tongue was progressing eastward, and prevented the most humid air from reaching the LMTA. A related contributing factor to the difference in rainfall between the two cases occurred late in the two IOPs as the cold fronts (on the western edge of the moist tongues seen in Figs. 2c-d) progressed from west to east of the Alps (Fig. 1a). In IOP2B, retardation of the low-level cold front's eastward progress produced strong conditional instability in the LMTA, and consequently, an additional episode of convective rain there. In IOP8, the prefrontal air in the Po Valley was so cold that the retardation of the cold front produced little change in the pre-existing large static stability and hence there was no additional period of convective rain. Finally, we use the simulations to show how unblocked (IOP2B) versus blocked (IOP8) flow on the scale of the Po Valley (Fig. 1b) explains the differences between IOP2B and IOP8 in small-scale orographic flow modifications observed with multi-Doppler radar in the LMTA (Fig. 1c).

Section 4 contains a summary and outlook for further analysis of the MAP SOP data.

2. Observations

The days of heaviest rain in northern Italy for IOP2B and IOP8 were 20 September 1999 and 21 October 1999, respectively. By coincidence, the passage of the rain-inducing synoptic-scale features (Fig. 2) occurred at nearly the same time of day in both cases, and so the present comparative analysis will be done through side-by-side presentations of data from IOP2B and IOP8 at the same hour UTC (as done in Fig. 2).

(*a*) *Rainfall*

The rainfall accumulated over the relevant 24h period for both cases is shown in Figs. 3a-b. Comparing Figs. 3a and 3b shows that there was much more rain on the Alpine

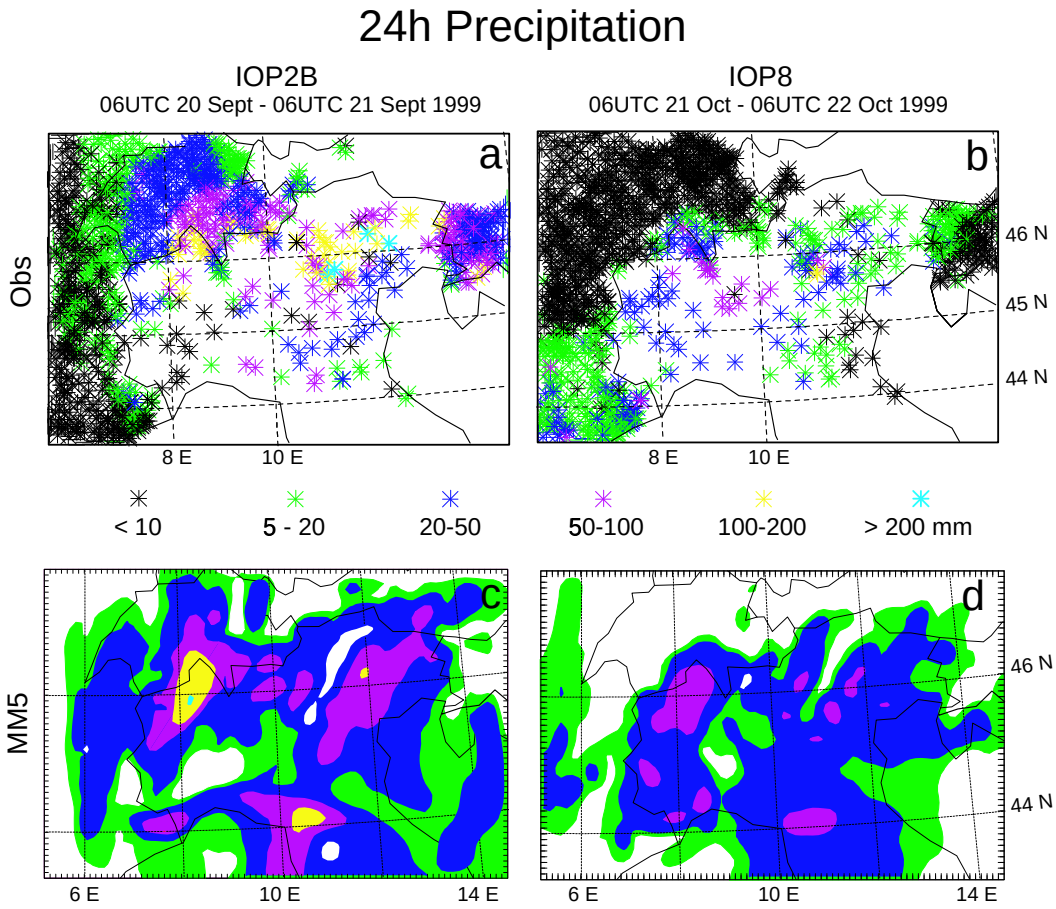

Figure 3. 24h accumulated precipitation for a) IOP2B (observed), b) IOP8(observed), c) IOP2B (simulated) and d) IOP8 (simulated) on Domain 2 (Fig. 1b). Color code for the simulations follows that indicated for the observations.

south side (roughly along 46N) in IOP2B than there was in IOP8. The comparison also shows that there is considerable rain north of the Alpine ridge line (Fig. 1b) in IOP2B, but almost none there in IOP8. In and near the LMTA (Fig. 1c), rainfall is weak and widespread over the western Po Valley in IOP8, while in IOP2B it is intense and localized

to the Alpine south side. (Included here in Fig. 3 for ease of comparison are results from numerical simulations which will be described below.)

Figure 4 shows the radar-derived precipitation rate from the Monte Lema radar (Joss

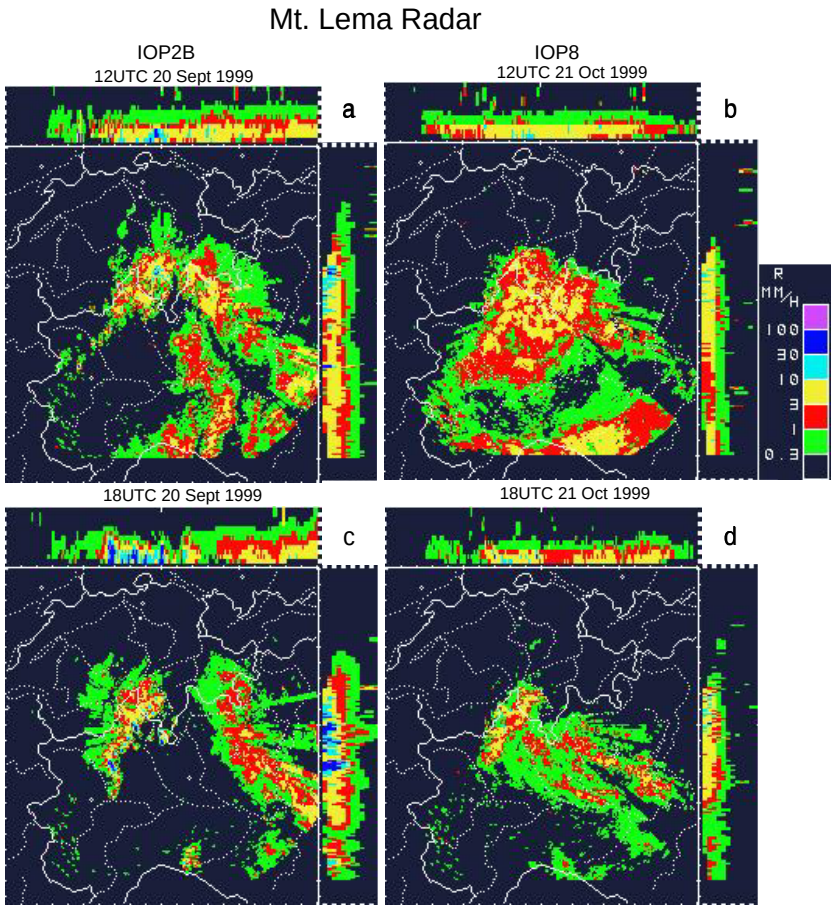

Figure 4. Best estimate of radar-derived precipitation rate from the Monte Lema radar on the domain indicated in Fig. 1b at 12UTC on a) 20 September 1999 (IOP2B) and b) 21 October 1999 (IOP8) and at 18UTC on c) 20 September 1999 and d) 21 October 1999. Rectangular plots at top and right side of each frame show maximum reflectivity in vertical cross-sections running west to east and south to north, respectively; the vertical scale in these is expanded by a factor of four (Joss *et al.* 1998, p. 54).

et al. 1998; location indicated in Fig. 1b; data available at http://www.map.ethz.ch) for selected times during the periods examined in Fig. 3. Examination of the entire sequence of five-minute-interval images (not shown) reveals that the rain-echo motion was basically southerly with the center of rain-echo mass gradually shifting eastward through the periods in both cases. There were, however, two significant differences between cases IOP2B and IOP8. In IOP2B, the early period was characterized by the most intense and persistent rainfall occurring up against the south-facing slopes of the Alps in the LMTA as shown in Fig. 4a. However for the early period of IOP8, the most intense and persistent rainfall occurred south of the radar location over the Po Valley, as shown in Fig. 4b. This picture is re-reinforced by examination of the rain-gauge data (Fig. 3a-b) in the LMTA. The other significant difference between the two cases was the occurrence

of deep convection late in the period along the southeast-facing slopes of the Alps in IOP2B (Fig. 4c), but there was no such occurrence in IOP8 (Fig. 4d).

(*b*) *Thermodynamics and Airflow*

Figure 5 contains maps of temperature, dew-point depression, and wind information

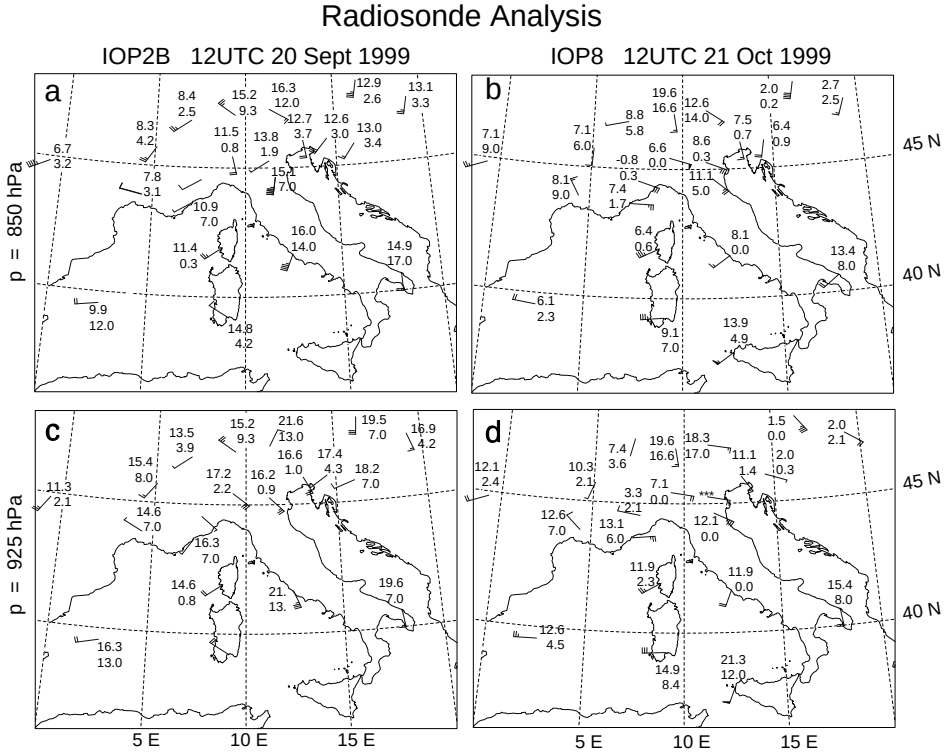

Figure 5. Radiosonde analysis at 12UTC at $p = 850$ hPa on a) 20 September 1999 (IOP2B) and b) 21 October 1999 (IOP8) and at $p = 925$ hPa on c) 20 September 1999 and d) 21 October 1999. Temperature and dew-point depression given at stem of wind flag; one full barb = 5 m s^{-1}.

from a combination of special and routine radiosonde observations made at 12UTC on 20 September 1999 and 21 October 1999, respectively. The two levels shown (925 and 850 hPa) were selected because they are generally below the Alpine ridge line (Fig. 1b) and give a good indication of the different orographic flow modification occurring in the two cases. Focusing on the Po Valley stations, there is in IOP2B southeasterly flow at 925 hPa (Fig. 5c) veering to southerly at 850 hPa (Fig. 5a), while in IOP8 the flow is east-southeasterly at both levels (Figs. 5b,d). The latter observations together with the terrain map in Fig. 1b indicate low-level flow in the Po Valley was much more across than along the Alpine ridge line in IOP2B than it was in IOP8. Observations made with the Meteo-France wind profiler at Lonate, Italy (Fig. 6; location marked in Fig. 1c) show that these two distinct flow patterns persisted throughout the respective IOPs. Consistent with the more-terrain-contour following flow in IOP8, Fig. 5 indicates the presence of a relatively cold stable air mass in the Po Valley in IOP8, but not in IOP2B. The soundings at Milan at 12UTC (Figs. 7a-b) show that in IOP2B the atmosphere directly upwind of the LMTA was nearly saturated and moist neutral up to about 400

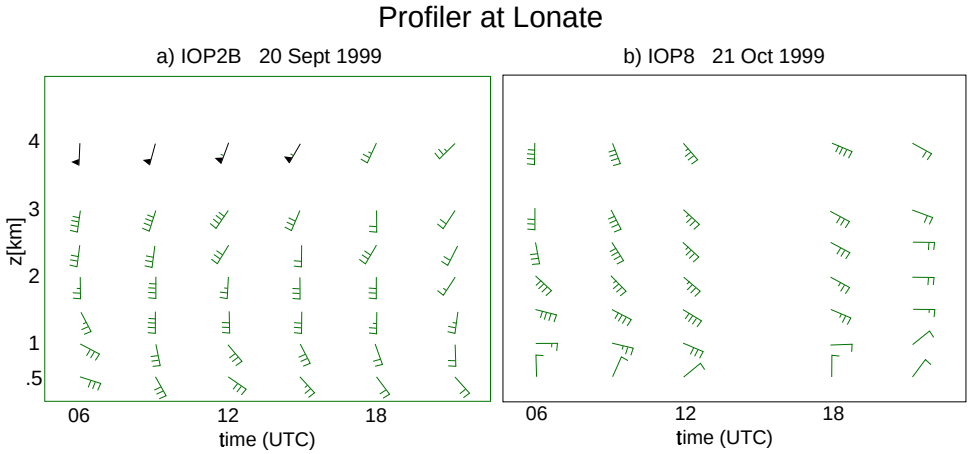

Figure 6. Winds derived from the Meteo-France windprofiler located at Lonate (see Fig. 1c) for a)20 September 1999 (IOP2B) and d) 21 October 1999 (IOP8). One full barb = 5 m s^{-1}.

hPa; while in IOP8 the sounding indicated saturated nearly moist neutral conditions above 900 hPa but with a stable (nearly isothermal) layer below.

The windprofiler observations in Fig. 6b indicate further that there was a weak northerly component of the wind at low levels in IOP8. Dropsondes made south of Genoa (Fig. 1b) near 08UTC 21 October 1999 [Fig. 9 of Bousquet and Smull (2002)] indicate northerly flow of cold stable air below 2 km, suggesting that the low-level easterly flow in the Po Valley (Figs. 5b,d) followed the terrain around to the south and to the Gulf of Genoa. This interpretation is consistent with the airborne Doppler analysis shown in Fig. 7a of Bousquet and Smull (2002).

By 00UTC 21 September 1999 in IOP2B, the Milan sounding shown in Fig. 7c indicates significant destabilization through cooling of the middle troposphere. The conditional instability evident in Fig. 7c is consistent with the strong convective cells observed in the LMTA later in IOP2B (Fig. 4c). In contrast, the sounding at 00UTC 22 October 1999 in IOP8 (Fig. 7d) shows that stable conditions persisted through the period.

3. Simulations and Analysis

(*a*) *Numerical Simulations*

Numerical simulations of cases IOP2B and IOP8 have been done with the Penn State/National Center for Atmospheric Research (PSU/NCAR) nonhydrostatic primitive-equation model known as the MM5 (Dudhia 1993; Grell *et al.* 1994). The model configuration was basically the one used by Rotunno and Ferretti (2001; RF) except here we use 29 unequally spaced vertical levels with the lowest model level being approximately 20 m above the ground. In this study we employ the three two-way nested domains as shown in Fig. 1; the coarse-grid domain (Domain 1, $\Delta x = 30$ km) is centered over Europe, an intermediate domain is used over the Alps and northern Italy (Domain 2, $\Delta x = 10$ km), and a high-resolution domain is positioned so as to include the LMTA (Domain 3, $\Delta x = 3$ km). A moist convection parameterization (Kain and Fritsch 1993) is used only for Domains 1 and 2, while only the explicit microphysics scheme of Dudhia (1993) is

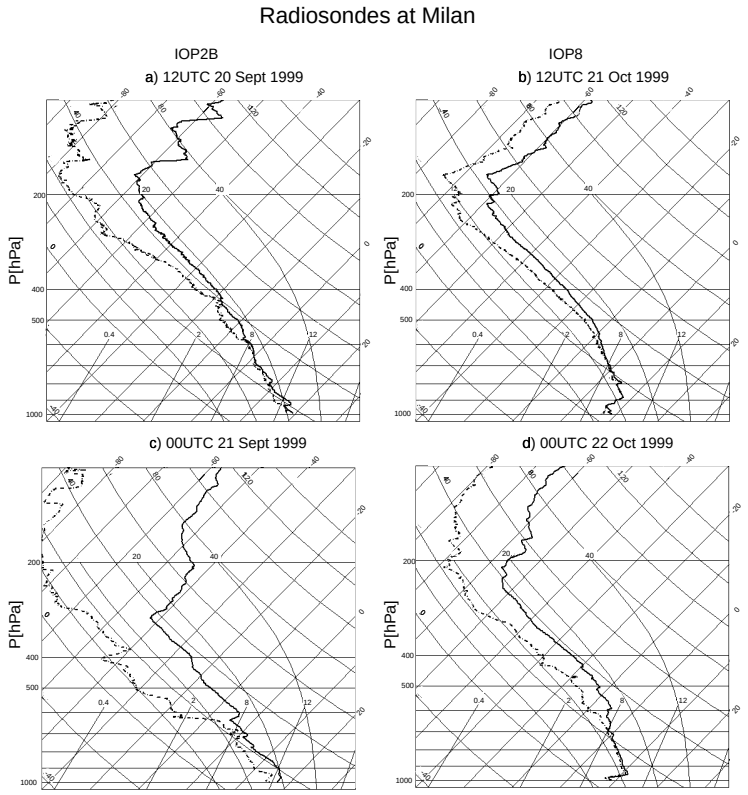

Figure 7. Skew T - log P charts from radiosondes ; launched from Milan (Fig. 1c) at 12UTC for a) 20 September 1999 and b) 21 October 1999 and at 00UTC for c) 21 September 1999 and d) 22 October 1999. Solid and dashed lines correspond to temperature and dew-point, respectively.

used on Domain 3. On all three domains, the planetary-boundary-layer parameterization known as the MRF scheme (Troen and Mahrt 1986; Hong and Pan 1996) is used. The European Center for Medium-Range Weather Forecast (ECMWF) analyses with 0.5 degree resolution are used to initialize the model and to upgrade the boundary conditions on Domain 1 every 6h. The simulation performed for IOP2B starts at 12UTC 19 September 1999 and that for IOP8 starts at 12UTC 20 October 1999 and both last for 48h.

The simulated feature of most interest here is the precipitation distribution and intensity. Figures 3c-d show the simulated 24h accumulated precipitation for IOP2B and IOP8, respectively. On the whole the simulations correctly distinguish the heavier-rain IOP2B from the lighter-rain IOP8; they also correctly produce rain north of the Alpine ridge line in IOP2B but not in IOP8. In both cases, the simulations underestimate the precipitation maximum in northeastern Italy. As in the observations for IOP2B (Fig. 3a), the simulations show the absence of precipitation in the western Po Valley (Fig. 3c); the simulation of IOP8 (Fig. 3d) shows more widespread rain in the western Po Valley as was observed (Fig. 3b) (although the simulation still tried to produce a local minimum there which was not evident in the observations).

Although the simulations do not agree in every way with the precipitation data, they

do capture the main difference of heavy (IOP2B) versus light (IOP8) rain, and so, can help explain that difference. In the following two sections we look at the principle rain-producing features of the respective IOP simulations, comparing them with the data already presented as appropriate, to uncover the reasons for the difference in rainfall between IOP2B and IOP8.

(*b*) *Analysis*

Figure 8 is constructed to illustrate the rain-producing features of the simulated flow in and near the LMTA (Fig. 1c) at 12UTC 20 September 1999 (IOP2B, left column) and 12UTC 21 October 1999 (IOP8, right column), which are near the times of maximum rain rate in each simulated case. In each column there are maps of equivalent potential temperature θ_e and airflow at $z = 3.0$ (Figs. 8a,b) and 0.75 km (Figs. 8c,d) from Domain 2 (Fig. 1b); also included on the $z = 0.75$ km maps are contours of rainfall accumulated from the beginning of the simulation; Figs. 8e,f show, respectively, air-parcel trajectories through the location of maximum rainfall (indicated by the 'T') in each case.

In the IOP2B simulation (Figs. 8a,c), the θ_e field can be described as a narrow, deep tongue of high values pushing northward into the Po Valley from the Gulf of Genoa (Fig. 1b); at $z = 0.75$ km (Fig. 8c) there is convergence between the southerly flow associated with the high-θ_e tongue and the lower-θ_e air flowing almost parallel to the terrain, much as was the case in simulations of the Piedmont case of 4-5 November 1994 (see Fig. 7 of RF). Figures 8a,c show that even as the main axis of the tongue is advected eastward at $z = 3.0$ km (i.e. there is low-θ_e advection at 'S'), the easterly flow in the Po Valley keeps high-θ_e flowing into the LMTA; with the advection of low-θ_e at z =3.0 km (Figs. 8a) and high-θ_e at $z = 0.75$ km (Fig. 8c), there develops a tendency for θ_e to decrease with height in the LMTA.

As in the IOP2B simulation, the θ_e field at $z = 3.0$ km in the IOP8 simulation (Fig. 8b) can be described as a narrow tongue of high-θ_e values pushing northward into the Po Valley; however, at $z = 0.75$ km, Fig. 8d shows the presence of very low-θ_e air in the western Po Valley which appears to have prevented the entrance of low-level high-θ_e air from the Gulf of Genoa. The low-θ_e air in the Po Valley flows parallel to the terrain contours (Fig. 8d) as in the IOP2B simulation (Fig. 8c), however in IOP8 the easterly flow continues to follow the terrain contours and flows toward the south near (8E,45N). Figure 8d shows that significant rainfall occurs where the northerly flow from the Po Valley meets the moist air in the Gulf of Genoa near (8.5E,44.5N). As in the IOP2B simulation, Figs. 8b and 8d show that at $z = 3.0$ km there is low-θ_e advection at 'S' (Fig. 8b) while the easterly flow at $z = 0.75$ km high-θ_e air flowing into the LMTA (Fig. 8d). However in the IOP8 simulation, this differential advection of θ_e is not strong enough to produce conditional instability

To substantiate the foregoing description of the airflow based on static images and to appreciate the different orographic effect on rain rate in the IOP2B and IOP8 simulations, we show here air-parcel trajectories passing through the region of maximum rain rate in the LMTA. For each case, we consider the history of air parcels that at 12UTC are at the geographical location of maximum rainfall and at the three altitudes, 1.5, 2.25, and 3.0 km above sea level (local terrain height is approximately 1 km above sea level). For the IOP2B simulation, Fig. 8e shows that all three parcels start at low levels and then rise up and over the Alps and flow northward at respective altitudes 4.1, 4.0 and 5.1 km. For the IOP8 simulations (Fig. 8f) the parcel at T at the lowest-level (1.5 km) starts 6h earlier at $z = 0.35$ km in the Po Valley as in the IOP2B simulation (Fig. 8e), however in IOP8 the parcels rides up the southeastward-facing slopes, but then descends back into the Po Valley; the middle parcel (2.25 km) enters Domain 2 at $z = 0.88$ km, follows the

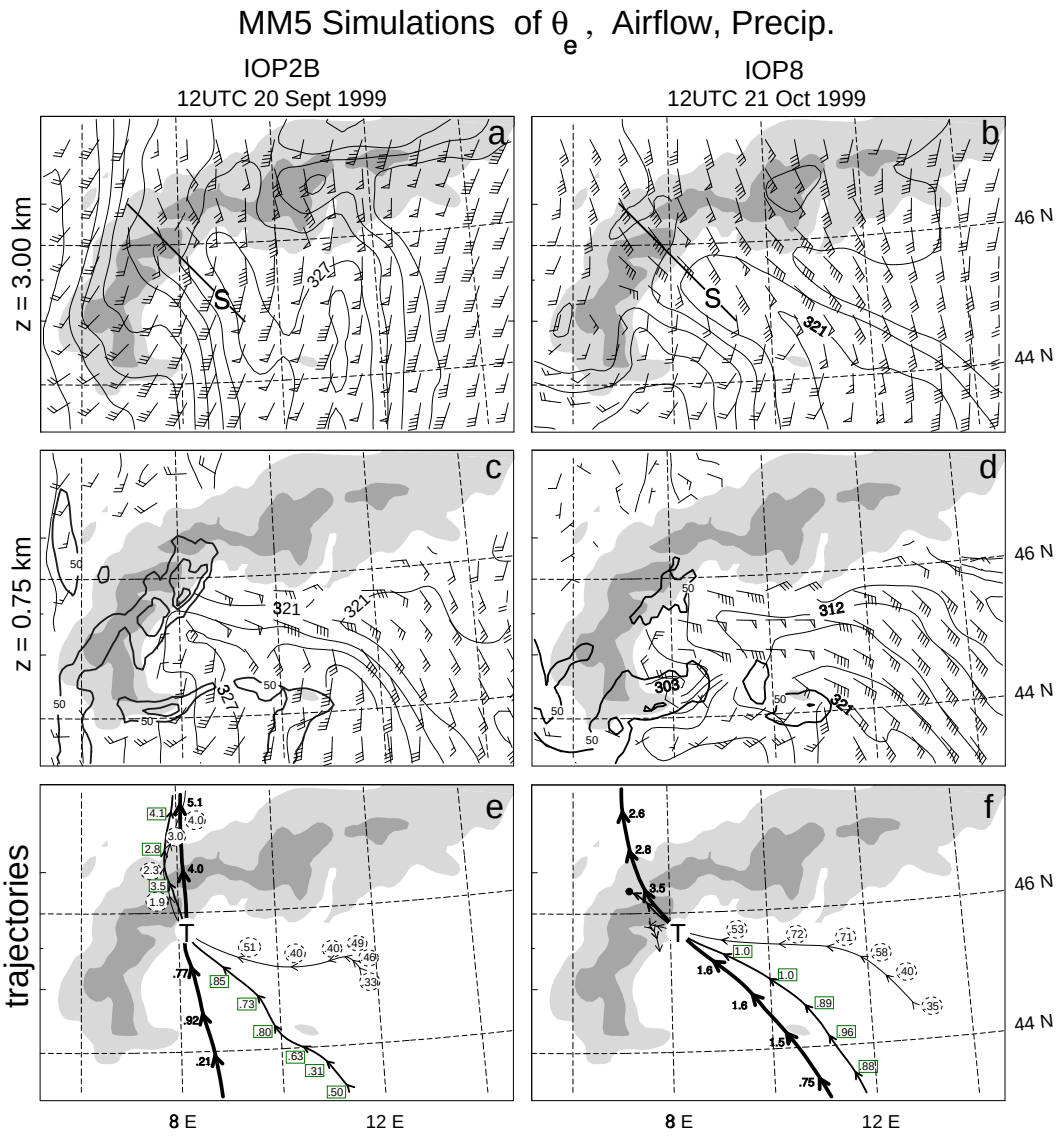

Figure 8. Simulated θ_e (c.i. = 3K) and wind (barb = 5 m s^{-1}) at 12 UTC at $z = 3.0$ km for a) IOP2B and b) IOP8, at $z = 0.75$ km for c) IOP2B and d) IOP8, and air-parcel trajectories for e) IOP2B and f) IOP8; precipitation accumulated over the simulation (c.i. = 50 mm) is indicated on the $z = 0.75$ km maps. Line and 'S' in a) and b) indicate locations of vertical cross-sections shown in Fig. 9 and soundings shown in Fig. 10. 'T' marks location of the air parcels at 12UTC whose trajectories are plotting forward and backward from $z = 1.5$ km (thin lines), $z = 2.25$ km (medium lines) and $z = 3.0$ km (thick lines); height (in km) given every hour and sense of flow given by the arrows.

terrain up and over the Alpine ridge line, and then enters a stagnation zone (indicated by the dot) two hours after it was at T; the third parcel (3.0 km) enters Domain 2 at $z = 0.75$ km, rides up and over the Alpine ridge line, but then descends to 2.6 km as it flows northward on the lee side. Hence the ascent of air parcels was much weaker in IOP8 than in IOP2B near the rainfall maximum. We will return to this point below in

the discussion of the factors contributing the difference in stable upslope rainfall between IOP2B and IOP8.

To illustrate the time-evolving upslope flow in the LMTA, we show in Fig. 9 vertical

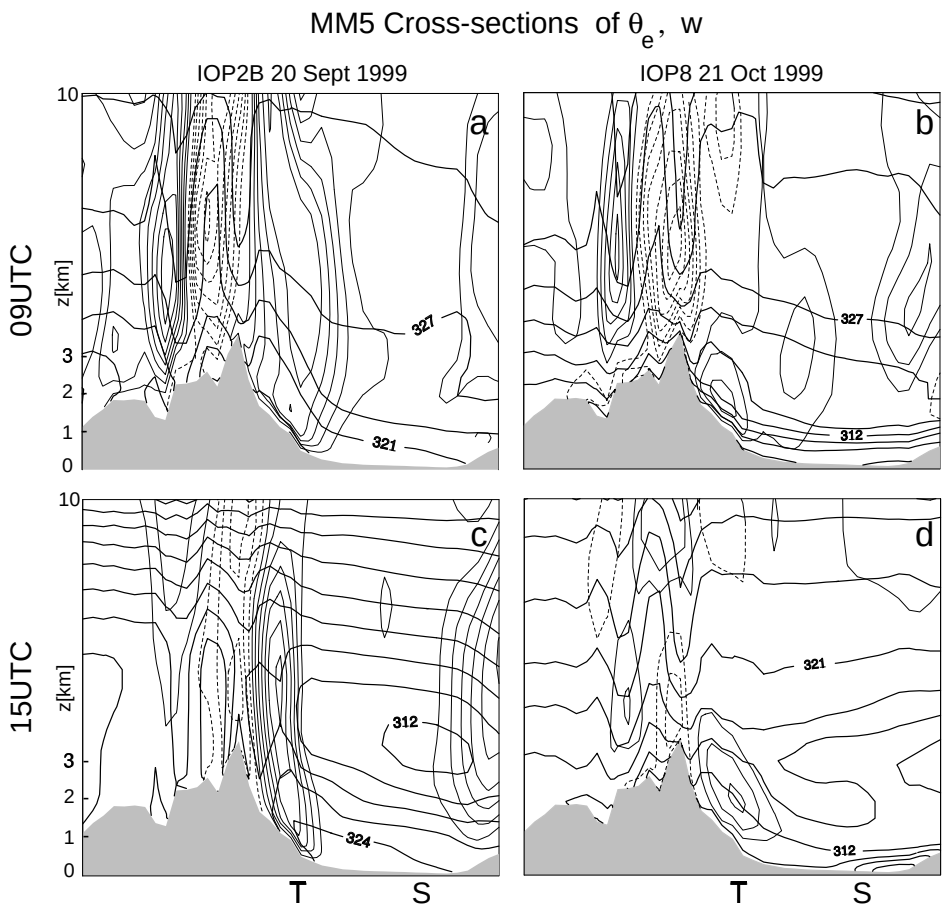

Figure 9. Cross-sections (indicated in Figs. 8a,b) of θ_e (c.i. = 3K) and w (c.i. = 0.2 m s^{-1}, dashed lines indicate negative values; zero line not plotted) at 09UTC for a) IOP2B and b) IOP8 and at 15UTC for c) IOP2B and d) IOP8. 'T' and 'S' correspond to the points indicated in Fig. 8

cross-sections (positions indicated by lines in Figs. 8a and 8b) of θ_e and vertical velocity w through the region of maximum rainfall, and in Fig. 10, local upwind soundings (positions indicated by the 'S' in Figs. 8a-b,9c-d) at 09UTC and 15UTC for each IOP simulation. For the IOP2B simulation, Fig. 9a indicates rising motion associated with locally upslope flow (Figs. 8a,c) that is producing the rain in that location; the local upwind sounding (Fig. 10a) shows that the flow feeding the rain maximum is nearly moist neutral. The elevated maximum of w (associated with the convergence of high- and low-θ_e air streams noted above) occurring in a nearly moist neutral atmosphere is again very similar to simulations of the 1994 Piedmont case (Figs. 8b,9b of RF). As inferred above from Figs. 8a,8c, Figs. 9c,10c show that the atmosphere has become locally conditionally unstable; the elevated maximum in w seen in Fig. 9c is now clearly associated with convective overturning. As in the IOP2B simulation, Fig. 9b shows the rising motion associated with

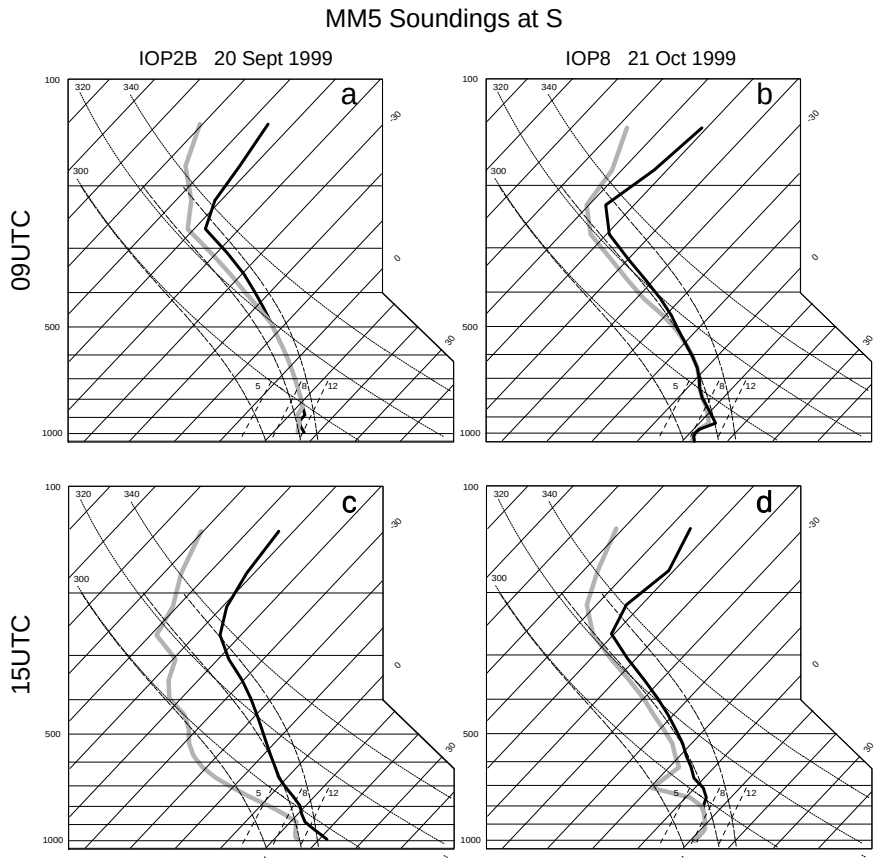

Figure 10. Simulated soundings at the points labeled 'S' in Figs. 8,9 at 09UTC for a) IOP2B and b) IOP8 and at 15UTC for c) IOP2B and d) IOP8. Dark and light lines correspond to temperature and dew-point respectively.

locally upslope flow that is producing the rain in that location; however in IOP8 there is a strong stable layer upon which the moist air rides. (There is even slight sinking motion on the terrain, as demonstrated in Fig. 8f). The local upwind sounding in Fig. 10b shows that the flow feeding the rain maximum is nearly moist adiabatic above approximately 900 hPa but very stable (nearly isothermal) below. Unlike the IOP2B simulation at 15 UTC, Figs. 9d and 10d show that in the IOP8 simulation the atmosphere continues to be locally stable.

Overall the MM5 simulations agree with the data shown in Section 2. As in the observations, the simulations produce more rainfall in the LMTA in IOP2B than in IOP8 (Fig. 3). For IOP2B both observations and simulations indicate that early in the period the air flowing into the LMTA was moist neutral (cf. Fig. 7a with 10a) and veered with height there from southeasterly to southerly (cf. Figs. 5a,c,6a with Figs. 8a,c); late in the period both observations and simulations indicate a locally unstable atmosphere (cf. Fig. 7c with Fig. 10c) and convection (cf. Fig. 4c with Fig. 9c). For IOP8B both observations and simulations indicate that the air flowing toward the LMTA was moist neutral above 900 hPa, but very stable (nearly isothermal) below (cf. Fig. 7b with Fig.

10b); wind-profiler observations (Fig. 6b) and trajectory analysis of the IOP8 simulation (Fig. 8f) agree that air from the lowest kilometer or so was blocked from rising over the Alpine barrier. In the following subsection we show why the low-level flow blocking in IOP8 made the difference between heavy and moderate simulated rain in the LMTA.

(c) *Difference in Rainfall between IOP2 and IOP8*

The rainfall at a location is by definition the rain rate $R(t)$ integrated over the duration. Figure 11 shows $R(t)$ at location T (indicated in Figs. 8e-f,9c-d). In the IOP2B

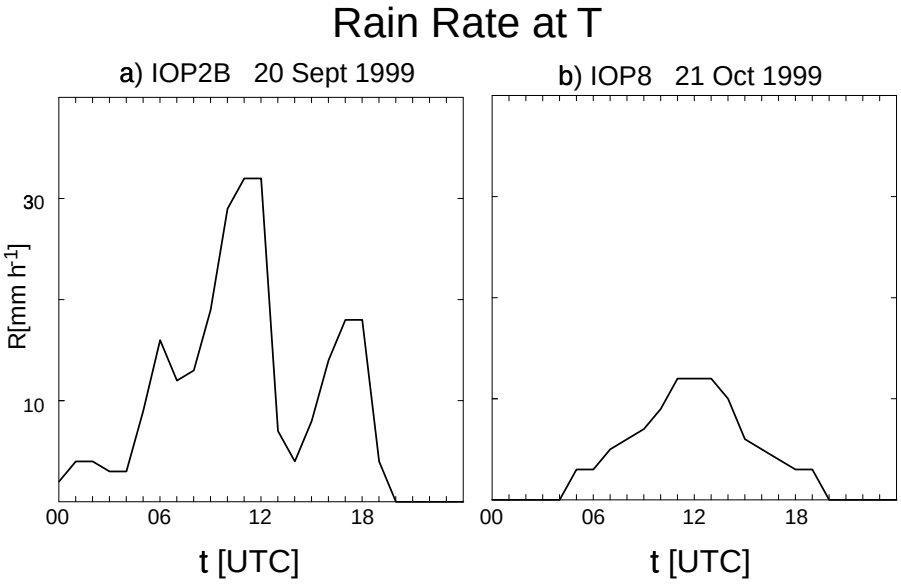

Figure 11. Rain rate versus time at the location 'T' indicated in Figs. 8,9 for a) IOP2B and b) IOP8.

simulation (Fig. 11a), the rain rate has two periods of intense rainfall: as discussed above, the first period is associated with moist neutral upslope flow (Figs. 9a,10a), while the later period is associated with convection (Figs. 9d,10d). In the IOP8 simulation (Fig. 11b) there was just the one period of stable upslope rain (Figs. 9b,d,10b,d); during this period, the IOP8 simulations exhibits values of R which are much less than they are in IOP2B.

As developed by Smith (1979), the simplest model for stable upslope rain is given by

$$R = \int_h^\infty -w \frac{\partial \rho_{vs}}{\partial z} dz \quad , \tag{1}$$

which comes from assuming that the rain rate R at the ground level, h, is given by the vertically integrated condensation rate, with the latter approximated by the vertical advection of saturation vapor density, ρ_{vs}. Figure 12 shows vertical profiles of w and ρ_{vs} at the place labeled T in Figs. 8-9 at 11UTC, which was near the time of maximum rate in IOP2B and IOP8. To the right of each figure is the contribution R_Δ to R for each 500m layer starting from $z = 1$ km. Summing the R_Δ gives $R \approx 47$ mm h^{-1} for IOP2B and $R \approx 17.2$ mm h^{-1} for IOP8. The actual maximum values near T in the simulations are

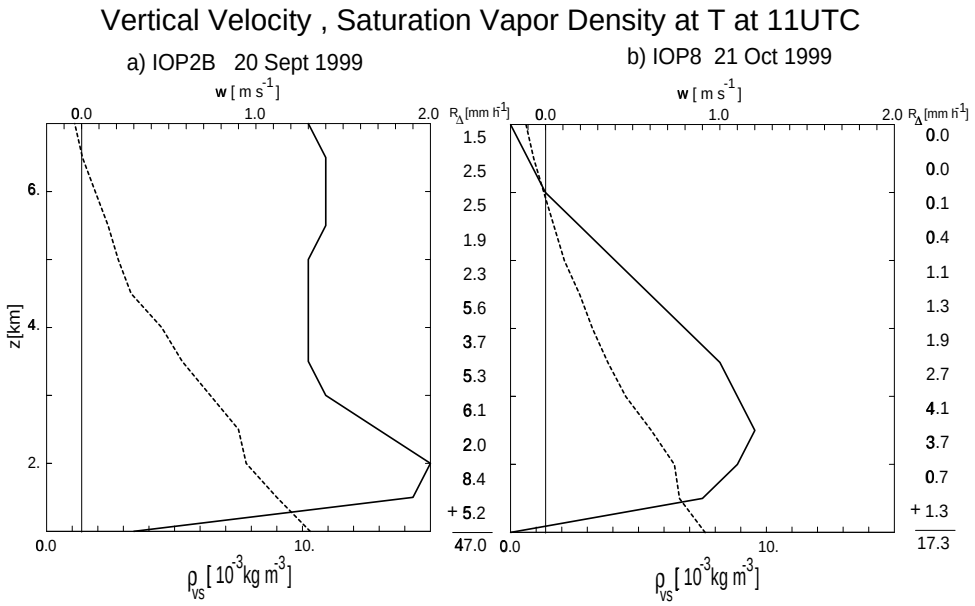

Figure 12. Vertical profiles of w (solid line),ρ_{vs} (dashed line) at location 'T' indicated in Figs. 8,9 at 11UTC for a) IOP2B and b) IOP8.

$R \approx 36$ mm h^{-1} and $R \approx 13$ mm h^{-1}, respectively. Since horizontal transport of liquid water is neglected in its derivation, one expects that (1) might overestimate the rain rate; this is particularly true in IOP2B given the strong winds at upper levels (Figs. 2a and 6a). Its overestimation of R notwithstanding, the computation of R from (1) does distinguish the larger-rain-rate IOP2B from the smaller-rain-rate IOP8. The layer-by-layer contributions to (1) shown in Fig. 12 indicate that the low-level stability in the IOP8 simulation substantially reduced both w and $|\frac{\partial \rho_{vs}}{\partial z}|$ over the lowest 1-2 km, thus reducing R.

One further relevant comparison can be made between the IOP8 simulation, and RF's simulation of the Piedmont flood of 4-5 November 1994. The thermodynamic conditions in both cases are similar above 900 hPa at the upstream sounding location (cf. Fig. 10b with RF's Fig. 9b), however without the blocked layer in the 1994 Piedmont case, both w and $|\frac{\partial \rho_{vs}}{\partial z}|$ were substantially larger, and consequently, larger rain rates were simulated. However even if the rain rate of the IOP8 case had been comparable to that of the 1994 Piedmont case, the duration time of the IOP8 event (Fig. 11) was much shorter, and hence the total rainfall in IOP8 would still have been much less than that of the 1994 Piedmont case.

(*d*) *Orographic Flow Modification*

The foregoing simulations of the different orographic flow modifications occurring in each case allows explanation of some puzzling Doppler-radar observations. Figures 13a,c show the Doppler-derived winds* in the LMTA for a period during which stable upslope rain was occurring in IOP2B and IOP8, respectively. In IOP2B (Fig. 13a) the

* Shown in Fig. 13 are the real-time products and quality control of the raw data is yet to be done (R. Houze, personal communication). We note however that the real-time analysis in Fig. 13 is consistent with the more rigorous single-Doppler analysis shown in Fig. 14 of Medina and Houze (2002).

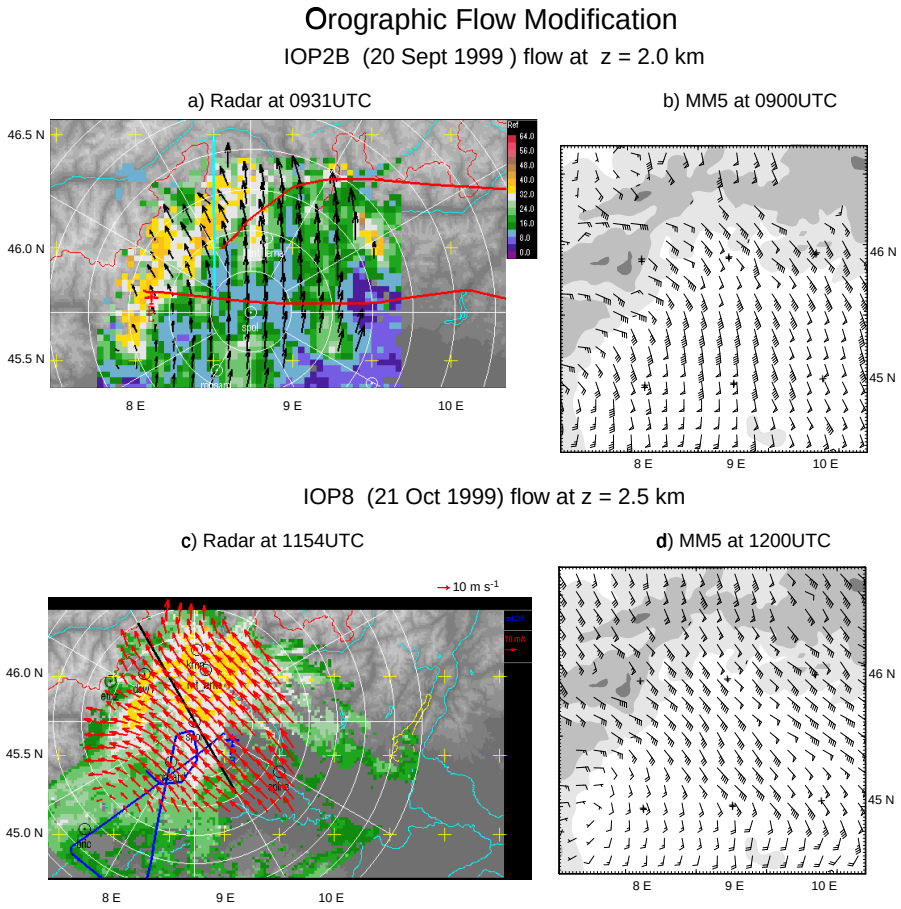

Figure 13. Comparison of orographic flow modification on Domain 3 (Fig. 1c) from simulations of a) IOP2B at $z = 2.0$ km at 09UTC 20 September 1999 and of b) IOP8 at $z = 2.5$ km at 12UTC 21 October 1999. Times, locations and levels chosen to correspond to those of observational analysis. Radar images available in the MAP Field Catalog, POC Science Coordinator Notes, http://www.map.ethz.ch.

Doppler-derived winds at $z = 2.0$ km indicate southerly flow south of the radar and with southeasterly flow associated with the rain echoes on the southeastern-facing slopes of the Alps. In IOP8 (Fig. 13c) the Doppler-derived winds at $z = 2.5$ km indicate southeasterly flow appearing to split and flow north and west of the massif running roughly north from Mt. Rosa (7.8E,45.9N; cf. Fig. 1c) to the Bernese Alps (with the highest peaks near 8.0E, 46.3N; cf. Fig. 1c). Comparison with the simulations from Domain 3 in Figs. 13b and 13d, respectively, indicates that the model has captured the different orographic flow modification. The trajectory analysis of Figs. 8e-f and the flow fields in Figs. 8a-d suggest a simple explanation: In IOP2B air parcels at the $z = 2.0$ km level ascend from below carrying southeasterly momentum to a level where the ambient wind is southerly. In IOP8 low-level air never rises to the $z = 2.5$ km level; the stable southeasterly flow

coming towards the above-described massif splits and flows around towards the north and the west.

4. Discussion and Summary

The data, supplemented by the present numerical simulations, indicate that as in previous cases of intense rain on the Alpine south side, events are set into motion by a synoptic-scale trough that brings a supply of moist air towards the Alps (Massacand *et al.* 1998). As demonstrated in a number of recent numerical studies the Piedmont flood of 4-6 November 1994 (Buzzi *et al.* 1998; Ferretti et al. 2000), suppression of orography significantly reduces total rainfall indicating that synoptic-scale lifting is not the essential mechanism producing flooding rain. These studies have also demonstrated that the mesoscale effect of latent heating is crucial as it allows the synoptic-scale southerly flow to surmount the tall Alpine barrier and so produce copious rain on the Alpine south side. Doswell *et al.* (1998) noted that the intense rain leading to the 1994 Piedmont flood occurred under locally convectively stable conditions; RF found that, moreover, the atmosphere was nearly moist neutral and they exploited this fact in considering simplified models of orographically modified moist airflow.

RF showed that the distinctive low-level flow pattern of southerly flow converging with westward-deflected flow along the Alpine south side (see their Fig. 7c) can be attributed to the nearly zero moist stability of the southerly flow (which suffers little deflection by the Alpine barrier) meeting the more-statically stable, westward-deflected air in Po Valley. In both the IOP2B simulation and RF's simulation of the 1994 Piedmont case, the low-level air coming from the east is more stable than that of the southerly stream it encounters, however it is not so stable as to prevent the low-level air from rising up and over the Alpine barrier, as demonstrated by the trajectory calculation in Fig. 8e. In IOP8 another element in the orographic flow modification came into play: a low-level air mass* so stable that the westward-deflected flow was unable to rise over the Alpine barrier, and instead followed the Alpine barrier until it flowed southward over the low point in the topography between the Maritime Alps and the Appenines [Fig. 1b, Fig. 7a of Bousquet and Smull (2002)]. We have provided evidence here that this stable layer reduced the condensation rate in the LMTA and so the rainfall rate associated with the stable upslope flow in IOP8 with respect to that in IOP2B.

The available evidence indicates that in IOP8 the deep stable layer in the Po Valley acted to lift moist air in the coastal zone of the Gulf of Genoa (Fig. 1b) and so acted to deplete the moisture from the air before it reached the LMTA. Observations (Fig. 3b) and the present simulations (Fig. 3d) indicate significant rainfall along the Maritime Alps. There were also pilot reports of thunderstorms south of the Appenines in the Gulf of Genoa whose remnants were apparently drifting northward into the LMTA network of radar observations (e.g. as in Fig. 4b) and producing widespread precipitation in the southwestern Po Valley (Fig. 3d). The generally higher altitude in IOP8 (as compared with IOP2B) of the trajectories feeding the rain-producing updraft in the numerical simulations (cf. Fig. 8f with Fig. 8e) is consistent with this interpretation.

Ferretti *et al.* (2002) show that during the southerly flow precipitation-related MAP IOPs, the forecasts over the Po Valley (on the lee side of the Appenines) were not as good as those for the south-facing Alpine slopes. Precipitation forecasts on the lee side of mountains is notoriously difficult (e.g., Colle and Mass, 2000). The cold stable layer

* Examination of the weather maps for the days preceding IOP8 indicates that the cold air in the Po Valley was of continental origin, entering from the Balkans.

of IOP8 may also present similar difficulties and is one of several effects we are currently investigating to understand the factors that limit the accuracy of precipitation forecasts in this region.

Acknowledgements

Comments on the first draft of this paper by C. Davis and S. Low-Nam of NCAR are gratefully acknowledged. The MAP archive and ITAMAP (Gruppo italiano raccolta dati MAP) are kindly acknowledged for the data. The second author thanks CETEMP (Centro di Eccellenza) for its partial support of this research.

References

Bougeault, P., Binder P., Buzzi, A., Dirks, R., Houze, R., Kuettner, J., Smith, R. B., Steinacker, R., and Volkert, H.	2000	The MAP Special Observing Period. *Bull. Amer. Met. Soc.*, **82,** 433–462
Bousquet, O. and Smull, B. F.	2002	Observations and impacts of upstream blocking during MAP IOP8. *Quart. J. Roy. Meteor. Soc.*, this volume
Buzzi, A., Tartaglione, N. and Malguzzi, P.	1998	Numerical simulations of the 1994 Piedmont flood: Role of orography and moist processes. *Mon. Wea. Rev.*, **126,** 2369–2383
Colle, B. A. and Mass, C. F.	2000	The 5-9 February flooding event over the Pacific Northwest: sensitivity studies and evaluation of the MM5 precipitation forecasts. *Mon. Wea. Rev.*, **128,** 593–617
Doswell, C. A., Ramis, C., Romero, R. and Alonso, S.	1998	A diagnostic study of three heavy precipitation episodes in the western Mediterranean region. *Wea. and Forecasting.*, **13,** 102–124
Dudhia, J.	1993	A nonhydrostatic version of the Penn State-NCAR mesoscale model: Validation tests and simulation of an Atlantic cyclone and cold front. *Mon. Wea. Rev.*, **121,** 1493–1513
Ferretti, R., Low-Nam, S., Rotunno, R.	2000	Numerical Simulations of the Piedmont flood of 4-6 November 1994. *Tellus*, **52A,** 162–180
Ferretti, R, Paolucci, T., Giuliani, G., Cherubini, T., Bernardini, L. and Visconti, G.	2002	Evaluation of the high resolution real-time forecast over the alpine region during the MAP experiment. *Quart. J. Roy. Meteor. Soc.*, this volume
Grell, G. A., Dudhia, J. and Stauffer, D. R.	1994	A description of the fifth-generation Penn State/NCAR Mesoscale Model (MM5). NCAR Tech. Note NCAR/TN-398+STR, 138pp. [Available from National Center for Atmospheric Research, P.O. Box 3000, Boulder, CO 80307.]
Hong, S.- Y., and Pan, H.- L.	1996	Nonlocal Boundary Layer Vertical Diffusion in a Medium-Range Forecast Model. *Mon. Wea. Rev.*, **124,** 2322–2339
Kain, J. S., and Fritsch, J. M.	1993	Convective parameterization for mesoscale models: The Kain-Fritsch scheme. *The representation of cumulus in numerical models, Meteor. Monogr.*, **46,** Am. Meteorol. Soc., 165–177

Joss, J., Schädler, B., Galli, G., Cavalli, R., Boscacci, M., Held, E., Della Bruna, G., Kappenberger, G., Nespor, V. and Spiess, R. 1998 *Operational Use of Radar for Precipitation Measurements in Switzerland.* VDF Hochschulverlag AG an der ETH, Zurich, 108 pp. (ISBN 3 7281 2501 6)

Medina, S. and Houze, R. A. 2002 Airmotions and precipitation growth in Alpine storms. *Quart. J. Roy. Meteor. Soc.* this volume

Rotunno, R. and Ferretti, R. 2001 Mechanisms of intense Alpine rainfall. *J. Atmos. Sci.*, **58,** 1732–1749

Smith, R. B. 1979 The influence of mountains on the atmosphere. *Advances in Geophysics*, **21,** 87–230

Troen, I., and Mahrt, L. 1986 A simple model of the atmospheric boundary layer; sensitivity to surface evaporation. *Boundary-Layer Meteor.*, **37,** 129–148